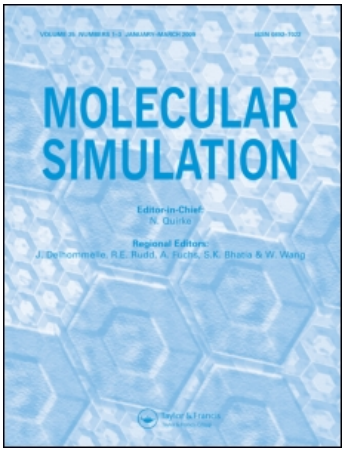

Molecular Simulation
Publication details, including instructions for authors and subscription information:
http://www.informaworld.com/smpp/title~content=t713644482

Molecular simulation of zinc oxide nanostructures confined in carbon nanotubes

Denis Horlait[a]; Benoit Coasne[a]; Aude Mezy[a]; Didier Ravot[a]; Jean-Claude Tedenac[a]
[a] Institut Charles Gerhardt, UMR 5253 CNRS, Université Montpellier 2, ENSCM, Place Eugène Bataillon, Montpellier Cedex 05, France

Online publication date: 24 November 2010

To cite this Article Horlait, Denis , Coasne, Benoit , Mezy, Aude , Ravot, Didier and Tedenac, Jean-Claude(2010) 'Molecular simulation of zinc oxide nanostructures confined in carbon nanotubes', Molecular Simulation, 36: 13, 1045 — 1058
To link to this Article: DOI: 10.1080/08927022.2010.501798
URL: http://dx.doi.org/10.1080/08927022.2010.501798

Molecular Simulation
Vol. 36, No. 13, November 2010, 1045–1058

Taylor & Francis
Taylor & Francis Group

Molecular simulation of zinc oxide nanostructures confined in carbon nanotubes

Denis Horlait, Benoit Coasne*, Aude Mezy, Didier Ravot and Jean-Claude Tedenac

Institut Charles Gerhardt, UMR 5253 CNRS, Université Montpellier 2, ENSCM, Place Eugène Bataillon, 34095 Montpellier Cedex 05, France

(*Received 5 April 2010; final version received 14 June 2010*)

This paper reports on a molecular simulation study of ZnO nanostructures confined within carbon nanotubes. Both the effects of confinement (by varying the pore size) and degree of pore filling (by varying the number of confined ZnO monomers) on the structure of the nanomaterial are addressed. None of the nanostructures exhibits the ideal structure of one of the ZnO bulk crystal phases (rocksalt, blende and wurtzite), but some crystalline features with significant correlations for the first and second nearest neighbours are observed. Close inspection of the location of the peaks in the pair correlation functions, of the angle distributions between Zn–O nearest neighbours and of some corresponding molecular configurations suggest that the confined nanoparticles possess mainly the local ordering of wurtzite. We also found evidence for defects such as Zn atoms that are involved in both a four-atom ring (characteristic of a cubic phase) and a six-atom ring (characteristic of wurtzite). Due to the smaller coordination number of atoms located at the interface between the nanostructure and the nanotube, the number of nearest neighbours of like and unlike atoms is smaller than that of the bulk. It is also found that the morphology of the nanostructures embedded in the carbon nanotubes depends in a subtle way on the different parameters involved in the synthesis (nanotube size, filling density). ZnO arranges itself to form either nanorods (quasi-1D systems) or an isolated nanoparticle (dimensionality 0D). When the filling density is low, further calculations suggest that the isolated particle is more well ordered and is more stable. We also show that the O atoms are polarised along the radial direction $\Delta r > 0$ (i.e. towards the external free interface). Our results also show that the use of a symmetrical nanopore as a template imposes that the confined particles exhibit surfaces terminated with both Zn and O atoms in the same stoichiometry.

Keywords: nanostructure; zinc oxide; carbon nanotube; semiconductor

1. Introduction

Among low dimensional semiconductors, zinc oxide (ZnO) nanorods are of special interest for their applications as high-efficiency short-wavelength optoelectronic nanodevices because of their large excitonic binding energy and high mechanical and thermal stabilities [1,2]. As a result, significant efforts have been made to the synthesis of nanostructured ZnO materials, due to their potential use for electronic, photonic, catalytic and sensor applications. As will be discussed in more detail below, one simple way to obtain ZnO nanostructures consists of using nanoporous materials or nanotubes as template. Among nanoporous solids that can be used for such processes, carbon nanotubes are important materials because of their simple geometry and uniform size [3,4]. From a fundamental point of view, carbon nanotubes are also considered as model materials to investigate the effect of nanoconfinement on the thermodynamic and dynamic properties of fluids. In particular, the cylindrical geometry of the tubes makes it possible to address in a simple way the effect of confinement on adsorption, capillary condensation and freezing/melting of fluids in nanopores. As a result, many experimental, theoretical and molecular simulation studies have been reported on the thermodynamics of fluids confined in these materials (for reviews, see [5,6]).

Reviews have been recently published on the synthesis of ZnO nanoobjects and their use [7–11] for fundamental and applied researches. From an experimental point of view, many methods, such as radio-frequency magnetron sputtering, chemical vapour deposition, spray pyrolysis, thermal evaporation and electrophoretic deposition, have been employed for the growth of ZnO nanomaterials [12–17]. As noted above, nanoporous materials used as a template provide also a simple way to obtain ZnO nanostructures. As a result, many porous materials zeolites [18,19], porous silicon [20], porous alumina [21,22], porous carbons [23], porous silicas (micelle-templated porous materials) [24–30] have been used to prepare ZnO nanostructures. Many of these studies revealed that the photoluminescence spectrum of nanoconfined ZnO is blue-shifted compared to the bulk [19,20,25,29] due to a larger amount of oxygen vacancies in the nanostructures. Of particular interest for the present work, some authors were able to demonstrate the formation of ZnO within the nanopores of a host porous material. Seo et al. [22] showed that ZnO nanotubes obtained within porous alumina have smooth wall morphologies and well-defined diameters

*Corresponding author. Email: benoit.coasne@enscm.fr

ISSN 0892-7022 print/ISSN 1029-0435 online

DOI: 10.1080/08927022.2010.501798
http://www.informaworld.com

after the removal by selective etching of the initial porous material. Schroder et al. [28] also demonstrated the formation of ZnO nanostructures within MCM-48 by the disappearance of free Si-OH group at the surface of the porous material. From a liquid precursor, Polarz et al. [31] obtained mono-dispersed ZnO nanoclusters in the pores of a MCM-48-like silica porous material. Molecular modelling of ZnO nanostructures confined in nanopores has received considerably less attention. To our knowledge, Jentys and Grimes [32] were the first to study ZnO embedded in a nanoporous material; using molecular simulation, these authors showed that ZnO confined in zeolite induces significant distortions that cause energy penalties. More recently, Kulkarni et al. [33,34] have used molecular dynamics and first-principle calculations to study the stability of ZnO nano-objects and found evidence for a novel phase transformation in ZnO nanowires from wurtzite to a graphite-like hexagonal structure. Such a new surface-driven phase transition (for a recent review on confinement effect on crystallisation, see also [6]) might occur in confined systems and are, thus, of particular relevance for studies on materials embedded in porous matrices. More recently, we have also reported a molecular simulation study of ZnO nanostructures confined in cylindrical silica nanopores of various sizes. In this previous work, we studied (1) the stability of ideal crystal phases confined in silica pores and (2) the nanostructures obtained from cooling down a confined homogeneous ZnO liquid.

Despite the significant works described above, some uncertainties remain regarding the morphology and structure of confined zinc oxide nanostructures. In particular, because of the lack of conclusive experiments, characterisation of structural and morphological defects in the embedded zinc oxide nanostructures is needed. In the present work, we report on a molecular simulation study of ZnO nanostructures confined within carbon nanotubes. Such 'numerical experiments' provide useful insights into the behaviour of nanomaterials as they allow estimating microscopic properties that are not directly accessible in real experiments. The choice of carbon nanotube has been motivated by the fact that it corresponds to an ideal system having a well-defined geometry and that it possesses a diameter that can be easily varied. Moreover, carbon nanotubes are promising candidates for the synthesis of semiconductor nanostructures as they could be either removed (by selective etching of the carbon matrix without affecting the zinc oxide nano-object) or left as part of the composite system. The simulations of the ZnO nanomaterial confined in the nanotubes were carried out using the Monte Carlo (MC) algorithm in the canonical ensemble combined with a simulated annealing technique. We also report some additional free energy calculations to further test and characterise the stability of the nanoparticles. In order to shed light on the effect of confinement on the morphology and structure of the nanoparticles, we varied the nanotube size. We also addressed the effect of the density (by varying the number of confined ZnO monomers) on the dimensionality and crystallinity of the confined material. The latter point allowed us to discuss the effect of partial filling of the nanotube as it remains in most experimental studies an unknown parameter. Along the same line, we also considered the effect of the filling of the nanotube by comparing the results obtained (1) when the initial pore filling is homogeneous along the pore axis (initial liquid ZnO nanocylinder) and (2) when the pore filling is heterogeneous (an initial nanodroplet of ZnO is prepared within the nanotube). The structure of the confined material was analysed using pair correlation functions, which were compared with those for ideal ZnO crystal structures (wurtzite, rocksalt and blende). The crystalline order of the nanoparticles was also investigated using geometrical order parameters such as the angle distribution $P(\theta)$ between Zn–O nearest neighbours. The remainder of the paper is organised as follows. In Section 2, we briefly discuss the details of the simulation techniques. Sections 3 and 4 present the results of our atomistic simulations for ZnO confined in the carbon nanotubes. Section 5 contains concluding remarks and suggestions for future work.

2. Models and simulation method

2.1 Carbon nanotubes and intermolecular potentials

Single-wall carbon nanotubes were constructed from a graphite sheet according to the arm-chair mode of rolling. Two carbon nanotubes of diameter $D = 1.8$ and 2.6 nm were considered in this work in order to address the effect of confinement on the stability of ZnO nanostructures. The length of the nanotubes is 5.2 nm. ZnO was described in our simulations as ions interacting through pair potentials. The formal charges $+2$ and -2 were used for Zn and O, respectively. The interatomic potential energy is the sum of the dispersion interaction with a short-range repulsive contribution and the coulombic interactions. We used an analytical expression of the Buckingham type to describe the short-range repulsion and dispersion interactions between two species i and j (Zn or O):

$$U_{ij}(r_{ij}) = A_{ij}\exp(-b_{ij}r_{ij}) - \frac{C_6^{ij}}{r_{ij}^6}, \qquad (1)$$

where A_{ij}, b_{ij} and C_6^{ij} are the parameters of the repulsion–dispersion interaction, and r_{ij} is the distance between the ions i and j. We also used a core–shell potential [35] to account for the polarisability of the anion O^{2-}. In the core–shell model, each ion consists of a core of charge X and a shell of charge Y, such that the total charge is the sum of the core and shell charges (i.e. -2 for O^{2-}). The core and shell were connected by a harmonic spring having

Table 1. Parameters for potential functions and core-shell model for ZnO (data from [36]).

	A (eV)	b (Å^{-1})	C_6 (eVÅ^6)	k (eVÅ^{-2})
O_s-O_s	22764.000	6.711	27.880	
$Zn-O_s$	700.30	2.959	0.000	
O_c-O_s				74.92

Notes: O_c and O_s denote the core and shell of the anion O^{2-}, respectively. The charges of the core and the shell were $X = 0.86902e$ and $Y = -2.86902e$, respectively.

Table 2. Lennard-Jones potential parameters for Zn, O and C (data from Ref. [40]).

	Zinc oxide		
Atom	Zn	O	C
σ (nm)	0.4142	0.3232	0.3769
ε/k_B (K)	111.37	22.75	24.95

a constant k. The values for the potential parameters A_{ij}, b_{ij} and C_6^{ij} and the core–shell parameters X, Y and k were taken from the work by Lewis and Catlow on the calculations of lattice constant, elastic properties and dielectric constants for ZnO crystals [36,37]. Table 1 lists the model parameters representing the interatomic interactions for ZnO. The electrostatic interactions were calculated using the Ewald summation technique in order to correct the effect of the finite size of the simulation box. The Ewald parameter α was equal to 8.23 Å^{-1} and the k vectors were such that $|\vec{k}| \leq 7$ (these parameters were chosen according to the criteria proposed by Jackson and Catlow [38]). Interactions between the Zn and O atoms of zinc oxide and the C atoms of the carbon nanotubes were calculated using Lennard-Jones potentials (no Coulombian interaction was calculated due to the absence of partial charge on the C atoms of the carbon nanotube). The cross-species parameters Zn–C and O–C given in Table 2 were calculated through the Lorentz–Berthelot rules [39] using the parameters for like atoms reported by Partridge et al. [40].

2.2 *Canonical MC technique*

The MC technique in the canonical ensemble (NVT, where N, V and T are the number of particles, volume and temperature of the system) was used to simulate the formation of ZnO nanostructures at 300 K in the atomistic model of carbon nanotubes. This technique is a stochastic method that simulates a system having a constant volume V (the nanotube with the confined phase), number of particles N and temperature T [41–43]. Periodic boundary conditions were used along the nanotube axis so that the system is equivalent to a pore of infinite length. The ability of MC algorithms to reach equilibrium states in the case of solid structures is often limited by the difficulty of particles displacements in dense phases [44–46]. In order to overcome such metastability barriers, we combined the MC method with a simulated annealing technique. The latter being a minimisation technique that consisted of first melting at high temperature the structure to be optimised and then slowly lowering the temperature. Starting with an initial structure at high temperature ($T = 4600$ K, which is larger than the melting point of bulk ZnO), the system was run at this temperature for a large number of moves until it reached equilibrium; each move consisted either of randomly selecting and displacing a Zn or a O atom to a new position or of randomly displacing the core of a O atom. Then, the temperature was decreased and the system was again allowed to equilibrate; the difference between two successive temperatures was such that $T_{new} = 0.9T_{old}$. The simulation was complete when the temperature reached the ambient temperature $T = 300$ K. The use of a very high initial temperature enabled us to start with a homogeneous liquid of ZnO which was cooled down slowly to obtain well-equilibrated nanostructures within the pores. Of course, the carbon atoms were maintained fixed in the simulation to avoid the melting of the host material.

3. Structure and morphology of confined ZnO

We first investigated the effect of various parameters (pore size, filling density, etc.) on the morphology and crystallinity of ZnO nanostructures confined in carbon nanotubes. To do so, the pair correlation functions $g(r)$ obtained for the nanoparticles will be compared with those for ideal bulk ZnO crystals (wurtzite, rocksalt and blende) at 300 K which are shown in Figure 1. Both the Zn–O and Zn–Zn partial contributions are shown. It is worth noting that wurtzite is the stable phase for ZnO at ambient conditions [37,47]. We also report in Table 3 some properties for these ideal ZnO structures such as the lattice constants (a, c), the equilibrium volumes V_0 and the number and distance of neighbours of like atoms (AA) and unlike atoms (AB). Such numbers ($N_{1,AB}$ and $N_{2,AB}$) and distances ($d_{1,AB}$ and $d_{2,AB}$) of first and second nearest neighbours of Zn and O atoms can be used to distinguish the different crystal phases.

3.1 *Effect of pore size*

We first discuss the effect of the nanotube diameter on the structure and morphology of the confined ZnO nanoparticles. Figure 2 reports the pair correlation functions for ZnO embedded in the carbon nanotubes with $D = 1.8$ and 2.6 nm. Both the Zn–O and Zn–Zn partial contributions to the total $g(r)$ function are reported. The filling density was $\rho = \rho_0$, where ρ_0 is the density of particles in the bulk ZnO wurtzite crystal. None of the nanostructures exhibits the ideal structure of one of the ZnO crystals (rocksalt, blende and wurtzite). However, the nanostructures possess short-order crystalline features with significant correlations for the first and second nearest neighbours: (1) the first peak in the Zn–O

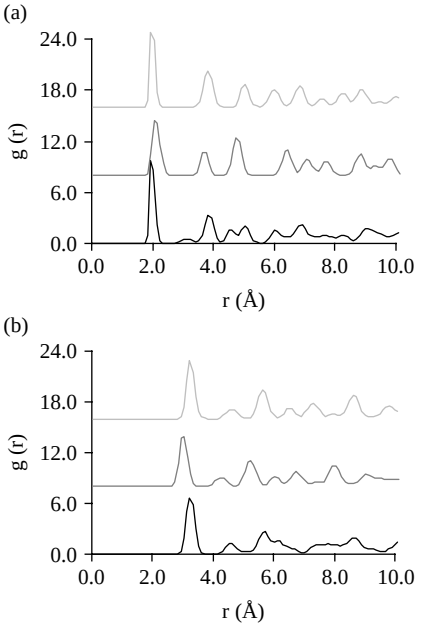

Figure 1. (a) Zn–O pair correlation function $g(r)$ for ideal bulk ZnO crystals at a temperature of $T = 300$ K: wurtzite (black line), rocksalt (dark grey line) and blende (light grey line) (colour online). For the sake of clarity, the pair correlation functions for the rocksalt and blende crystals were shifted by $+8$ and $+16$, respectively. (b) Same as (a) for the Zn–Zn pair correlation function $g(r)$.

Table 3. Some properties for common phases of ZnO: wurtzite (B4), rocksalt (B1) and blende (B3).

	Wurtzite (B4)	Rocksalt (B1)	Blende (B3)
V_0 (Å^3)	24.49	19.6	24.65
a (Å)	3.2960	4.28	4.62
c/a	1.580	–	–
$N_{1,\mathrm{AA}}$	12 (3.250)	12 (3.025)	12 (3.275)
$N_{1,\mathrm{AB}}$	4 (2.000)	6 (2.125)	4 (2.025)
$N_{2,\mathrm{AA}}$	6 (4.625)	6 (4.275)	6 (4.625)
$N_{2,\mathrm{AB}}$	1 (3.275)	24 (3.725)	12 (3.825)

Notes: Conventional lattice constants (a, c) are related to equilibrium volumes $V_0 = a^3/4$ (B1, B3) and $V_0 = \sqrt{3}a^2c/4$ (the latter volumes are different from the volumes of the unit cell). $N_{1,\mathrm{AA}}$, $N_{1,\mathrm{AB}}$, $N_{2,\mathrm{AA}}$ and $N_{2,\mathrm{AB}}$ are the number of first and second nearest neighbours of like atoms and unlike atoms, respectively (the number in parentheses is the corresponding distance in Å).

$g(r)$ function has a large amplitude (~ 6.8) compared to what is usually observed for liquids, (2) the second peak in the Zn–O $g(r)$ function is split into two secondary peaks and (3) the peaks are separated by almost zero minima. The first peak in the Zn–Zn $g(r)$ function also presents a shoulder on its left; as will be shown in Section 3.2, this shoulder corresponds to Zn atoms with four nearest neighbours, i.e. involved in a four-atom ring (while most of the Zn atoms possess six nearest O neighbours as in the wurtzite structure, i.e. are involved in six-atom ring). The local ordering of the ZnO nanostructures within the carbon nanotubes seemed

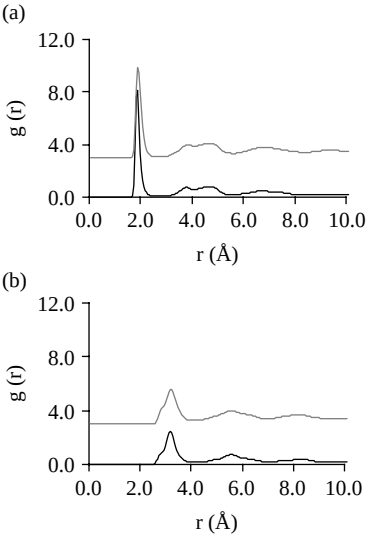

Figure 2. (a) Zn–O pair correlation function $g(r)$ for ZnO confined in a carbon nanotube: (black line) $D = 1.8$ nm, (grey line) $D = 2.6$ nm. The filling density was $\rho = \rho_0$ (see text). For the sake of clarity, the pair correlation functions for the carbon nanotube $D = 2.6$ nm have been shifted by $+3$. (b) Same as (a) for the Zn–Zn pair correlation function $g(r)$.

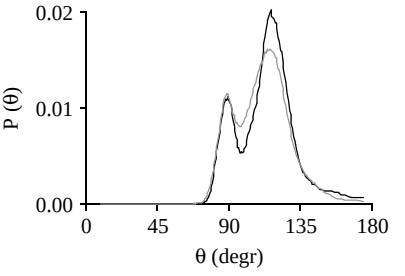

Figure 3. Angle distribution $P(\theta)$ between Zn–O nearest neighbours for ZnO confined in a carbon nanotube: (black line) $D = 1.8$ nm, (grey line) $D = 2.6$ nm. The filling density was $\rho = \rho_0$ (see text). The latter distributions have been averaged over 1000 typical configurations.

independent of the nanotube diameter as the pair correlation functions for $D = 1.8$ nm resemble those for $D = 2.6$ nm. This is confirmed by the results in Figure 3 showing that ZnO confined in the two nanotubes possess very similar angle distributions $P(\theta)$ between Zn–O nearest neighbours. Independent of the tube diameter, the angle distributions exhibit two peaks located at about 90° and 120°. This result shows that the confined nanostructures are made up of zinc atoms in a hexagonal environment (wurtzite-like) and zinc atoms in a cubic-like environment (blende-like or rocksalt-like). These different local environments can be seen in magnified views of the typical molecular configurations reported in Figure 4. We note that the local cubic environment observed in the simulated nanostructures corresponds to isolated four-coordinated ZnO monomers

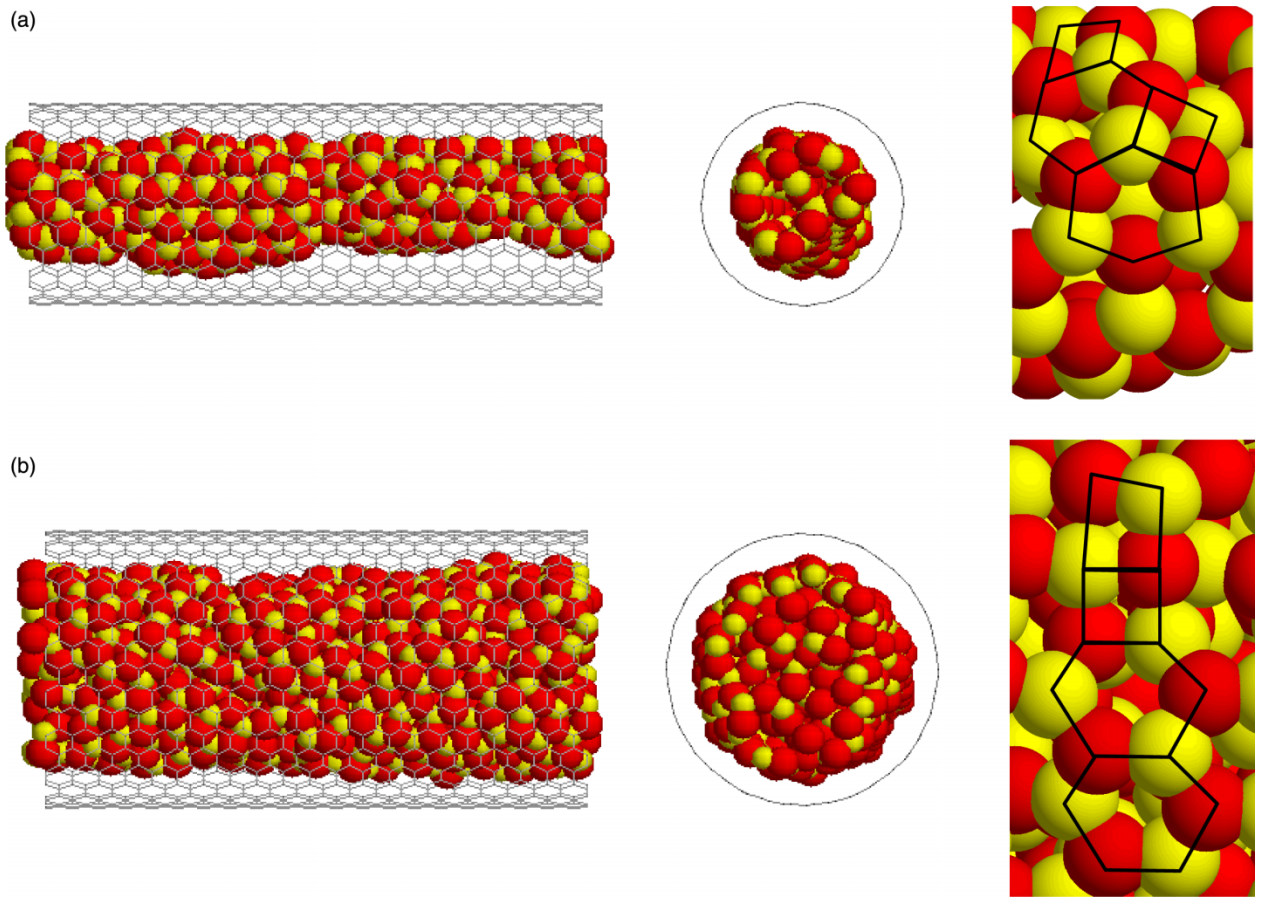

Figure 4. Transverse and cross-sectional views of ZnO nanostructures confined in a carbon nanotube: $D = 1.8$ nm (a) and $D = 2.6$ nm (b). The red and yellow spheres are the O and Zn atoms of ZnO, respectively. The grey sticks represent the C—C bonds of the carbon nanotube. The two extremities of the nanotube are connected to each other, due to the use of periodic boundary condition along the pore axis. For each system, a magnified view is shown on the right where one can see atoms in a hexagonal-like environment or cubic-like environment. The lines are provided as guide to the eye (colour online).

connected with hexagonal (wurtzite-like) ZnO units. Indeed, a peak located at $\theta \sim 180°$ would be observed if the cubic order observed in the angle distribution corresponded to blende or rocksalt domains. The positional pair correlation functions and angle distributions $P(\theta)$ obtained for the ZnO nanostructures in the carbon nanotubes cannot be identified unambiguously by comparing with those for ideal crystal structures. However, the location of the peaks for the Zn–O and Zn–Zn $g(r)$ functions, the maximum at about $\theta \sim 120°$ in the angle distributions $P(\theta)$, and the hexagonal ordering observed in the molecular configurations in Figure 4 suggest that the confined nanoparticles possess mainly the local ordering of wurtzite. This result is consistent with our previous molecular simulation study, in which we found that wurtzite embedded in silica nanopores was more stable than blende and rocksalt [48].

From the pair correlation functions in Figure 2, we estimated the number of first nearest neighbours of like atoms ($N_{1,\mathrm{AA}}$) and unlike atoms ($N_{1,\mathrm{AB}}$) using the following relation:

$$N_{i,\alpha\beta} = 4\pi\rho \int_i r^2 g_{\alpha,\beta}(r)\,\mathrm{d}r, \qquad (2)$$

where $N_{i,\alpha\beta}$ denotes the number of ith nearest neighbours of atoms α and $\beta(\alpha, \beta =$ Zn or O). The integration in Equation (2) runs over the range of distances r corresponding to the ith neighbours. The density ρ was taken equal to ρ_0, i.e. the density of atoms in bulk ZnO wurtzite. The number and distance of first nearest neighbours of like atoms and unlike atoms for the nanoparticles obtained in the nanotubes with $D = 1.8$ and 2.6 nm are reported in Table 4. We found $N_{1,\mathrm{AA}} = 7.17$ and $N_{1,\mathrm{AB}} = 3.34$ for the nanotube with $D = 1.8$ nm and $N_{1,\mathrm{AA}} = 8.87$ and $N_{1,\mathrm{AB}} = 3.64$ for the nanotube with $D = 2.6$ nm. The fact that these numbers are smaller than those for the bulk ideal structures (Table 3) is due to the atoms located at the interface between the nanostructure and the nanotube which possess a smaller coordination number. This result also corroborates with the fact that

Table 4. Number of first and second nearest neighbours of like atoms and unlike atoms: $N_{1,AA}$, $N_{1,AB}$, $N_{2,AA}$ and $N_{2,AB}$ (the number in parentheses is the corresponding distance in Å).

	$D = 1.8$ nm				$D = 2.6$ nm			
	$0.3\rho_0$	$0.5\rho_0$	ρ_0	$0.3\rho_0^*$	$0.3\rho_0$	$0.5\rho_0$	ρ_0	$0.3\rho_0^*$
$N_{1,AA}$	4.99 (3.17)	6.52 (3.17)	7.17 (3.17)	5.57 (3.17)	7.55 (3.22)	8.12 (3.22)	8.87 (3.22)	8.24 (3.27)
$N_{1,AB}$	2.81 (1.87)	3.30 (1.87)	3.34 (1.87)	3.00 (1.87)	3.60 (1.87)	3.50 (1.87)	3.64 (1.77)	3.60 (1.77)

Note: The asterisks refer to the data for the heterogeneous pore filling (see text).

Table 5. Energies (eV) per ZnO for nanostructures obtained in carbon nanotubes with $D = 1.8$ and 2.6 nm filled with three densities $\rho = 0.3\rho_0$, $\rho = 0.5\rho_0$ and $\rho = \rho_0$ (the number in parentheses indicates the number of ZnO monomers for each nanostructure).

	$D = 1.8$ nm				$D = 2.6$ nm			
	$0.3\rho_0$ (51)	$0.5\rho_0$ (85)	ρ_0 (170)	$0.3\rho_0^*$ (51)	$0.3\rho_0$ (166)	$0.5\rho_0$ (277)	ρ_0 (544)	$0.3\rho_0^*$ (166)
Confined								
E	−38.7	−38.9	−39.0	−39.0	−39.0	−39.1	−39.1	−39.1
$E_{ZnO/ZnO}$	−38.6	−38.8	−38.9	−38.9	−39.0	−39.1	−39.1	−39.0
$E_{ZnO/CNT}$	−0.1	−0.1	−0.1	−0.1	−0.1	−0.1	−0.1	−0.1
F	−38.5	−38.8	−38.9	−38.7	−38.9	−38.9	−39.0	−38.9
Free								
$E_{ZnO/ZnO}$	−38.6	−38.8	−38.9	−38.8	−39.0	−39.1	−39.1	−39.0

Notes: The asterisks refer to the data for the heterogeneous pore filling (see text). For all systems, the total energy E as well as the ZnO–ZnO and ZnO–carbon nanotube contributions is shown. We also report the free energy F of the nanoparticle which was determined from the Hessian matrix (see text). The energy of the 'free' nanostructure which was relaxed after the removal of the host carbon nanotube is shown in the last line of the table.

these numbers are smaller for the nanotube with $D = 1.8$ nm than for the nanotube with $D = 2.6$ nm (as the ratio of surface atoms to volume atoms increases with decreasing the nanotube diameter). Table 5 reports the energies in eV per ZnO monomers for the nanostructures obtained in the nanotubes with $D = 1.8$ and 2.6 nm. We also report in Table 5 the free energy of the nanoparticle, which was obtained using the Hessian matrix as described in a previous paper [49]. For both systems, the total energy E as well as the ZnO–ZnO ($E_{ZnO/ZnO}$) and ZnO–nanotube ($E_{ZnO/CNT}$) contributions is presented. $E_{ZnO/ZnO}$ for the nanotube with $D = 2.6$ nm (~ -39.1 eV) is smaller (more attractive) than that for the nanotube with $D = 1.8$ nm (~ -38.9 eV). This result reflects that the surface to volume ratio decreases when the nanotube size increases or when the number of ZnO monomers increases. Finally, due to the non-ideal structure of the confined systems, the absolute value of $E_{ZnO/ZnO}$ for both nanotubes is smaller than that for ideal crystal phases, 39.5–39.7 eV [47]. Due to weak (only dispersive) attractive interactions with the carbon atoms of the nanotube, $E_{ZnO/CNT} \sim -0.1$ eV is very small compared to $E_{ZnO-ZnO}$. The relative stability between the two nanostructures is not changed when one looks at the free energy of the nanoparticle instead of the energy. This is due to the fact that the vibrational contribution (entropy + energy) to the total free energy is small ~0.04–0.1 eV/ZnO monomer, compared to the total energy. We note that the values reported above for the energy and free energy of the nanoparticles are consistent with what is usually found for solid phases; the energy is of the order of magnitude of kJ/mol while the entropy is of the order of magnitude of J/mol. These values are also consistent with the work by Shen et al. [49] who found that the free energy lowering ($T\Delta S$) between a ZnO nanotube and nanowire composed of the same number of atoms is about $10\,k_BT$ (~0.02 eV/ZnO monomer).

3.2 *Effect of filling density*

We now discuss the effect of the filling density (i.e. the ratio of the number of ZnO monomers to that when the nanotube was filled with the density of wurtzite, ρ_0) on the structure and morphology of the confined nanoparticles. Such an investigation of the effect of the filling density on the structure and morphology of confined ZnO nanoparticles was motivated by the experiments by Polarz et al. [31] who found that most samples contain nanoparticles that are much smaller than the pore size; i.e. even if the pore is entirely filled by the liquid reactants, the synthesised ZnO nanoparticles do not fully occupy the porous space. Figure 5 shows the pair correlation functions for ZnO embedded with different filling densities in the carbon nanotubes with $D = 1.8$ and 2.6 nm. The three following filling densities were considered: $\rho = 0.3\rho_0$, $\rho = 0.5\rho_0$ and $\rho = \rho_0$. A filling density ρ means that the total pore volume V is filled with a number of atoms $N = \rho V$. For all filling densities, the structure obtained after relaxing the system at 300 K does not exhibit crystalline features, although some significant correlations

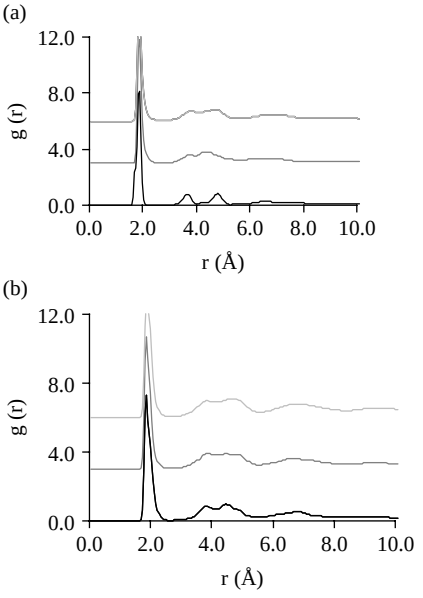

Figure 5. (a) Zn–O pair correlation function $g(r)$ for ZnO confined in a carbon nanotube with $D = 1.8$ nm for different filling densities (see text): (black line) $\rho = 0.3\rho_0$, (dark grey line) $\rho = 0.5\rho_0$ and (light grey line) $\rho = \rho_0$. For the sake of clarity, the pair correlation functions for $\rho = 0.5\rho_0$ and $\rho = \rho_0$ have been shifted by +3 and +6, respectively. (b) Same as (a) for ZnO confined in a carbon nanotube with $D = 2.6$ nm (colour online).

were observed for the first and second nearest neighbours. Interestingly, the particles exhibit more local ordering as the filling density decreases (the peaks in the $g(r)$ function becomes more marked with decreasing ρ). This result is due to the fact that the confined nanoparticle interacts less with the weakly interacting carbon atoms of the nanotube wall when ρ decreases (as it occupies a smaller fraction of the porous space). In the case of ZnO confined in silica pores, we found that the filling density does not affect the local ordering of the Zn and O atoms; it is believed that this is due to the Coulombian interactions between the atoms of the silica substrate and the Zn and O atoms that are quantitatively similar to those involved in the stability of ZnO.

We also show in Figures 6 and 7 typical molecular configurations of the ZnO nanostructures obtained for different filling densities in the carbon nanotubes with $D = 1.8$ and 2.6 nm, respectively. In the case of the nanotube with $D = 2.6$ nm, we found that ZnO forms nanorods (quasi-1D systems) for all filling densities. However, the nanostructure exhibits dispersion in its diameter along its axis as the filling density ρ decreases. In contrast to these results for the large nanotube, the morphology of the nanostructure in the case of the nanotube with $D = 1.8$ nm depends on the filling density of the porosity. ZnO arranges itself to form nanorods (quasi-1D systems) for $\rho = 0.5\rho_0$ and ρ_0, while a nanoparticle (dimensionality 0D) is observed for $\rho = 0.30\rho_0$. In the latter case, the nanostructure was composed of (1) a nanoparticle that spreads over the diameter of the nanopore and (2) a chain of ZnO atoms that connects the nanoparticle through the left- and right-hand

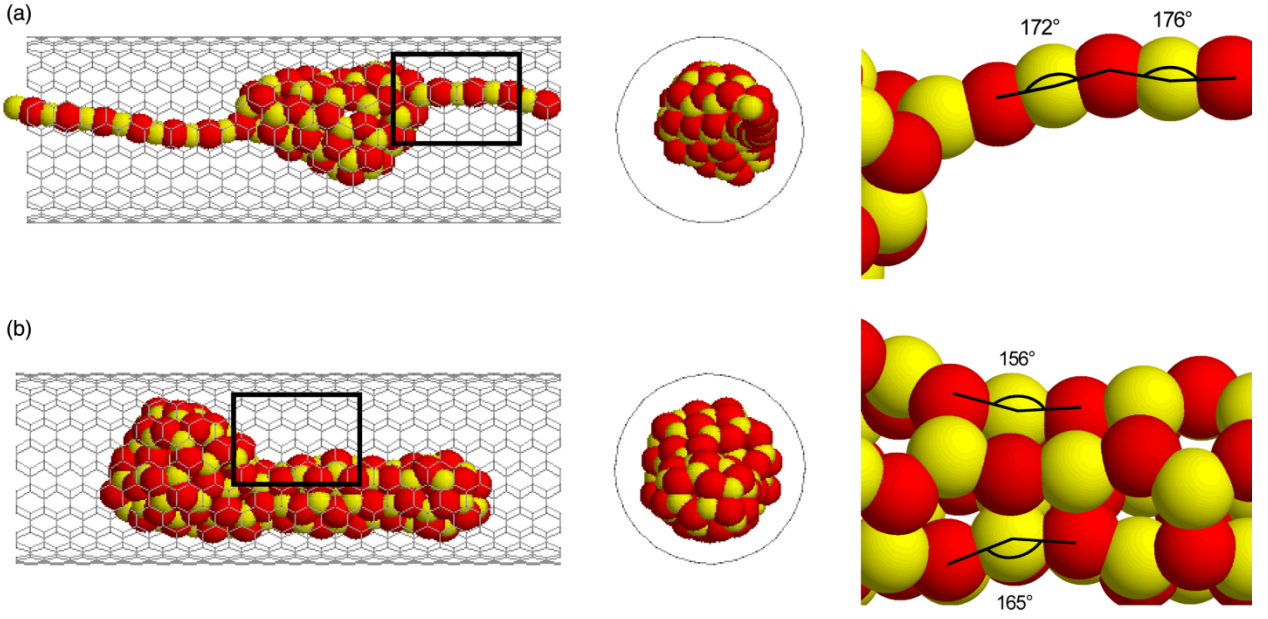

Figure 6. Transverse and cross-sectional views of ZnO nanostructures confined in a carbon nanotube with $D = 1.8$ nm filled with a density $\rho = 0.3\rho_0$ (a) and $\rho = 0.5\rho_0$ (b). The red and yellow spheres are the O and Zn atoms of ZnO, respectively. The grey sticks represent the C—C bonds of the carbon nanotube. The two extremities of the nanotube are connected to each other, due to the use of periodic boundary condition along the pore axis. For each system, a magnified view of the region indicated by the black rectangle on the left-hand side configuration is shown on the right with some characteristic angles.

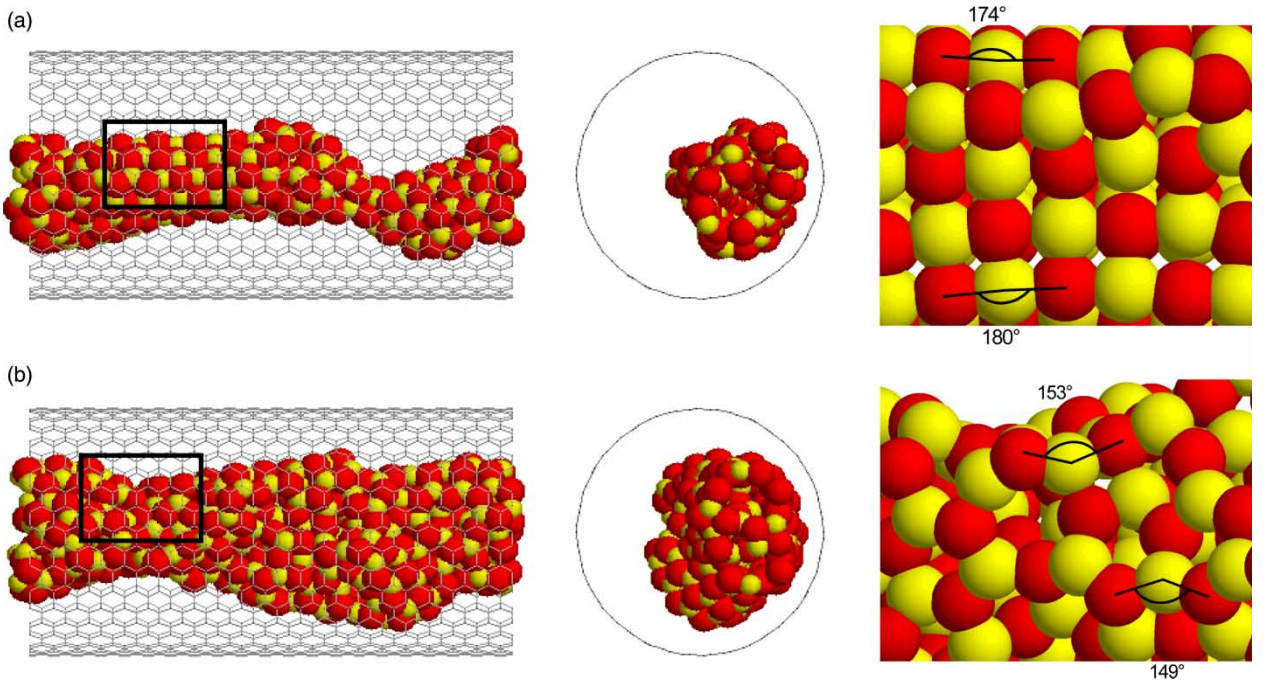

Figure 7. Transverse and cross-sectional views of ZnO nanostructures confined in a carbon nanotube with $D = 2.6$ nm filled with a density $\rho = 0.3\rho_0$ (a) and $\rho = 0.5\rho_0$ (b). The red and yellow spheres are the O and Zn atoms of ZnO, respectively. The grey sticks represent the C—C bonds of the carbon nanotube. The two extremities of the nanotube are connected to each other, due to the use of periodic boundary condition along the pore axis. For each system, a magnified view of the region indicated by the black rectangle on the left-hand side configuration is shown on the right with some characteristic angles.

sides of the simulation box (which are physically connected due to the use of periodic boundary conditions in the simulations). Such a defect (1D chain of atoms) is similar to those observed by Wilson in his study of KI confined in carbon nanotubes [50]. It must be emphasised that this defect, which is stable over the length of the simulation run, is probably metastable and would probably disappear to merge with the larger nanoparticle if longer simulation runs were performed. These observations on the dependence of the nanoparticle morphology on the nanopore size and filling density are similar to those reported in our previous work on ZnO confined in porous silicas [48].

In order to further characterise the local ordering in confined ZnO, we show in Figure 8 the distribution $P(\theta)$ of angles between Zn–O–Zn nearest neighbours for ZnO in the carbon nanotubes with $D = 1.8$ and 2.6 nm and for different filling densities. Again, for both nanotube diameters, the angle distribution exhibits two peaks which correspond, respectively, to zinc atoms in a hexagonal environment (wurtzite-like) and zinc atoms in a cubic-like environment (blende-like or rocksalt-like). The angle distributions obtained when the nanotubes are incompletely filled exhibit a third peak that is not observed with the largest density $\rho = \rho_0$ (Figure 3); independent of the nanotube diameter, this third peak is located at about $\theta \sim 180°$ and $\theta \sim 165°$ for the filling densities $\rho = 0.3\rho_0$ and $\rho = 0.5\rho_0$, respectively. In the case of the nanotube of a diameter $D = 1.8$ nm, the third peak $\theta \sim 180°$ observed

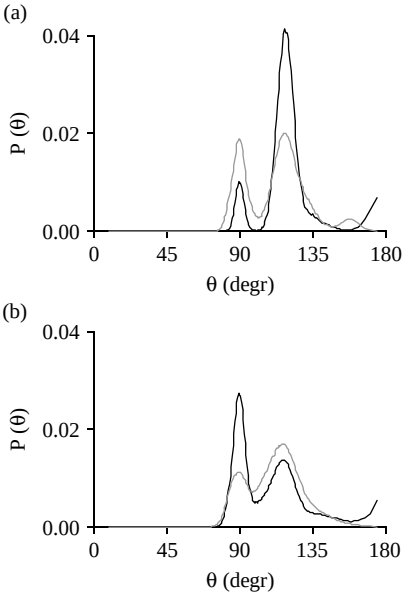

Figure 8. (a) Angle distribution $P(\theta)$ between Zn–O nearest neighbours for ZnO confined in a carbon nanotube with $D = 1.8$ nm: (black line) filled with a density $\rho = 0.3\rho_0$, (grey line) filled with a density $\rho = 0.5\rho_0$.The latter distributions have been averaged over 1000 typical configurations. (b) Same as (a) but for the nanotube with $D = 2.6$ nm.

for $\rho = 0.3\rho_0$ corresponds to the angle formed by the Zn and O atoms in the chain that connects the nanoparticle through the left- and right-hand sides of the simulation box (see the magnified view in Figure 6). In contrast, in the case of the nanotube of a diameter $D = 2.6$ nm, the third peak $\theta \sim 180°$ observed for the same filling density corresponds to Zn/O atoms that form nanodomains of a cubic symmetry (see the magnified view in Figure 7). In contrast to these results for the lowest filling density, the peak at $\theta \sim 165°$ in the angle distribution for the filling density $\rho = 0.5\rho_0$ in the nanotubes with $D = 1.8$ and 2.6 nm corresponds to Zn atoms that are involved in both a six-atom and four-atom rings (see the magnified views in Figures 6 and 7). The latter situation, which is also observed for the filling density $\rho = \rho_0$ (see the molecular configurations for $\rho = \rho_0$ in Figure 4), corresponds to a defect in which the Zn atom has to adjust between the hexagonal symmetry ($\theta \sim 120°$) and square symmetry ($\theta \sim 180°$).

The number and distance of first nearest neighbours of like atoms and unlike atoms for the nanoparticles obtained for different filling densities in the nanotubes with $D = 1.8$ and 2.6 nm are reported in Table 4. For both nanotubes, we found that $N_{1,AA}$ and $N_{1,AB}$ are significantly lower than those for the bulk structures (Table 3), due to the atoms located at the interface between the nanostructure and the carbon nanotube which possess a smaller coordination number. This result corroborates with the fact that these numbers increase with increasing the filling density (as the ratio of surface atoms to volume atoms decreases with increasing the number of ZnO monomers). Table 5 reports the energies in eV per ZnO monomers for the nanostructures obtained in the nanotubes with $D = 1.8$ and 2.6 nm. For both systems, the total energy E as well as the ZnO–ZnO ($E_{ZnO/ZnO}$) and ZnO–nanotube ($E_{ZnO/CNT}$) contributions is presented. $E_{ZnO/CNT} \sim -0.1$ eV, which is nearly independent of the nanotube size and filling density, is negligible compared to $E_{ZnO-ZnO}$. $E_{ZnO/ZnO}$ is both an increasing function of the nanotube diameter and the filling density. Again, this result is due to the fact that the surface to volume ratio decreases when the nanotube size increases or when the number of ZnO monomers increases. Finally, as noted above, the absolute value of $E_{ZnO/ZnO}$ for the nanoparticles is smaller than that for ideal crystal phases, 39.5–39.7 eV [47].

3.3 Effect of heterogeneous filling

The results reported in Section 3.2 suggest that the morphology of the ZnO nanostructures (nanorod or isolated nanoparticle) obtained within the nanotubes depends in a subtle way on the pore size and pore filling. In particular, it cannot be ruled out that the initial configuration used in the molecular simulations favour the formation of a particular morphology among these possible structures. In order to address this issue, we prepared in the case of the lowest filling density ($0.3\rho_0$) two different initial configurations of the nanoparticle: (1) a configuration in which the Zn and O atoms are randomly distributed within the nanotube and (2) a configuration in which the Zn and O atoms are randomly distributed in half of the porosity along the nanotube axis. In what follows, the former and latter cases will be referred to as homogeneous and heterogeneous fillings, respectively. We will also adopt the following notation: $0.3\rho_0$ for the nanoparticle obtained from the initial homogeneous filling and $0.3\rho_0^*$ for the nanoparticle obtained from the initial heterogeneous filling.

Figures 9 and 10 compare for ZnO embedded in the nanotubes with $D = 1.8$ and 2.6 nm the pair correlation functions obtained when starting with the homogeneous and heterogeneous initial configurations. We also report in Figure 11 typical molecular configurations of the resulting nanoparticles when the initial heterogeneous configurations were used. For both nanotubes, the ZnO nanoparticles form isolated nanoparticles when starting from the heterogeneous configurations. Close inspection of the molecular snapshots reveals that the particle obtained for the smallest nanotube is hollow; this result shows that the types of nanoparticles one can obtain using porous templates depend in a very subtle manner on the

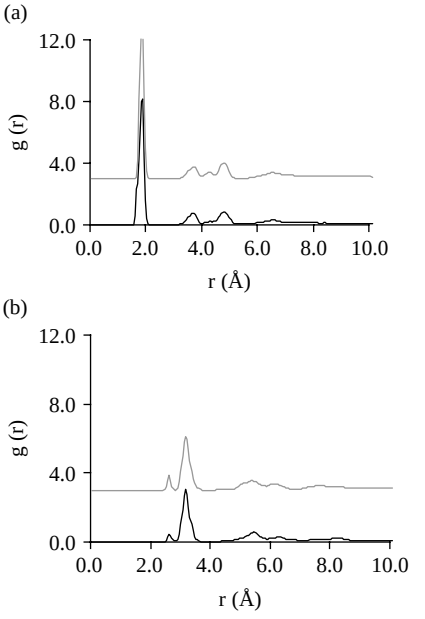

Figure 9. (a) Zn–O pair correlation function $g(r)$ for ZnO crystals confined in a carbon nanotube with $D = 1.8$ nm filled with a density $\rho = 0.3\rho_0$: (black line) homogeneous initial filling and (grey line) heterogeneous initial filling (see text). For the sake of clarity, the pair correlation functions for the heterogeneous initial filling were shifted by +3. (b) Same as (a) for the Zn–Zn pair correlation function $g(r)$.

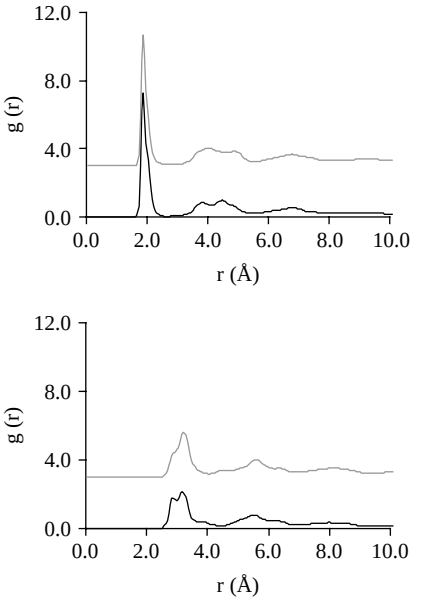

Figure 10. (a) Zn−O pair correlation function $g(r)$ ZnO filled with a density $\rho = 0.3\rho_0$: (black line) homogeneous initial filling and (grey line) heterogeneous initial filling. For the sake of clarity, the oair correlation functions for the heterogeneous initial filling were shifted by + 3. (b) Same as (a) for the Zn−Zn pair correlation function $g(r)$. confined in a carbon nanotube with $D = 2.6$ nm crystals.

synthesis conditions (pore size, pore filling, etc.). This result shows that the use of porous templates to obtain semiconductor nanoparticles is a versatile method leading to many interesting types of nanostructures that can be used for practical applications. For a given nanotube diameter, the pair correlation functions for the homogeneous and heterogeneous particles are very similar, which indicates that structural information gained from the pair correlation functions (or its experimental counterpart given by the inverse Fourier transform of the structure factor $S(Q)$) cannot be used to assess in a simple way the morphology of the nanoparticles.

The number and distance of first nearest neighbours of like and unlike atoms for the nanoparticles obtained for the heterogeneous filling are compared with those for the homogeneous fillings and are displayed in Table 4. Although the heterogeneous particle (isolated particle) possesses a larger surface to volume ratio than the homogeneous particle, its number of nearest neighbours of like and unlike atoms is larger. This result suggests that atoms in the heterogeneous particles are more well ordered than those in the homogeneous particle. A possible explanation is as follows. We found in a previous section that confined particles exhibit more local ordering as the filling density increases, due to the fact that they interact less with the weakly interacting atoms of the nanotube wall. In the case of the heterogeneous filling, the particles were indeed less in contact with the nanotube wall, which led to a better ordering of the ZnO particles. Such a better ordering was confirmed by the fact that the energy of the heterogeneous particle was lower (more attractive) than that of the homogeneous particle (see Table 5). Finally, this last result suggested that the

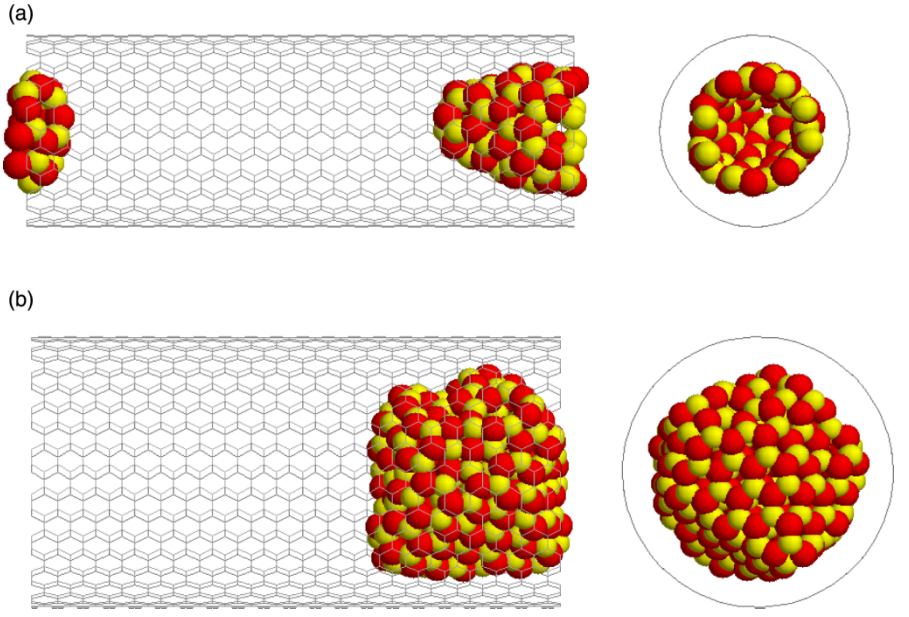

Figure 11. Transverse and cross-sectional views of ZnO nanostructures confined in carbon nanotubes initially filled with a heterogeneous density $\rho = 0.3\rho_0$: $D = 1.8$ nm (a) and $D = 2.6$ nm (b). The red and yellow spheres are the O and Zn atoms of ZnO, respectively. The grey sticks represent the C—C bonds of the carbon nanotube. The two extremities of the nanotube are connected to each other, due to the use of periodic boundary condition along the pore axis.

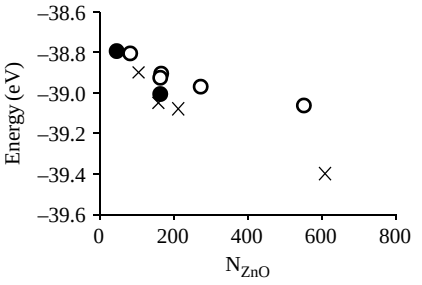

Figure 12. The white symbols are the energy (eV) as a function of the number of monomers ZnO for nanostructures obtained in carbon nanotubes with $D = 1.8$ and 2.6 nm filled with three densities $\rho = \rho_0$, $\rho = 0.5\rho_0$ and $\rho = 0.3\rho_0$. For all systems, the energy corresponds to the ZnO–ZnO contribution per ZnO monomer. The black symbols correspond to the energy of the nanostructure obtained by starting with a heterogeneous filling of the nanotubes, $\rho = 0.3\rho_0$ (see text). The crosses are the data from our previous work on ZnO nanostructures confined in silica pores.

homogeneous particle was metastable, while the heterogeneous particle was closer to the equilibrium configuration.

4. Stability and defects of confined ZnO

4.1 Energy

Table 5 reports the energies and free energies in eV per pair of ZnO atoms for the ZnO nanostructures obtained for all the confined nanoparticles considered in this work (two pore sizes, three filling densities, homogeneous versus heterogeneous fillings). We also report the energy of the 'free' nanostructures which have been relaxed after the removal of the host carbon nanotube. Due to the weak (only dispersive) attractive interactions between the carbon and the Zn and O atoms, the energy of the nanostructure after the removal of the host material is nearly equal to that of the embedded nanostructure. This result also corroborates with the fact that the Zn–O pair correlation functions $g(r)$ for the free structures (not shown) relaxed before and after the removal of the host material are almost identical. We also show in Figure 12 the contribution $E_{\mathrm{ZnO/ZnO}}$ as a function of the number of monomers ZnO for each nanostructure obtained in the present work. We also report previous data obtained for ZnO nanoparticles confined in silica nanopores [48]. Independent of the carbon nanotube diameter, $E_{\mathrm{ZnO/ZnO}}$ decreases (becomes more attractive) as the number of pairs of ZnO increases. Again, this result reflects that the surface to volume ratio decreases when the nanotube size increases or when the number of ZnO monomers increases. As previously mentioned, for a given number of ZnO monomers, the particles obtained from the heterogeneous filling of the nanotube were more stable than when the homogeneous filling was imposed. $E_{\mathrm{ZnO/ZnO}}$, which varies from -38.6 eV for the smallest density down to -39.1 eV for the largest density, remains larger than the typical energy per ZnO monomer in bulk ZnO (~ -39.4 eV). Finally, these results are consistent with our previous work on ZnO nanostructures confined in silica pores in which we found that the bulk-like behaviour was not recovered for particles with less than 600 ZnO monomers. In addition, our results suggest that the energy of the nanoparticles is independent of the substrate as the data for carbon nanotubes and silica nanopores almost fall on the same master curve when plotted as a function of the number of ZnO monomers (Figure 12).

4.2 Local ordering and dipole orientation

We now discuss in detail the local ordering of the nanoparticles obtained in the present work. As mentioned in the first section of this paper, the pair correlation functions and the number/distance of nearest neighbours cannot be used to characterise in an unambiguous way the structure of the ZnO nanoparticles. However, the combination of the location of the peaks for the Zn–O and Zn–Zn $g(r)$ functions, the angle distributions $P(\theta)$, and the hexagonal ordering observed in the molecular configurations suggest that the confined nanoparticles possess mainly the local ordering of wurtzite. As noted above in this paper, for each of the nanoparticles considered in this work, a subpeak in the first peak of the Zn–Zn $g(r)$ function is observed at a distance $d_{1,\mathrm{AA}} \sim 2.72$ Å. Depending on its relative amplitude, the latter peak appears either as a shoulder on the left of the main peak (Figures 2 and 10) or as a small isolated peak (Figure 9). In order to clarify the origin of this peak, we identified in several molecular configurations Zn atoms for which the Zn–Zn distance is smaller than 2.9 Å. In each

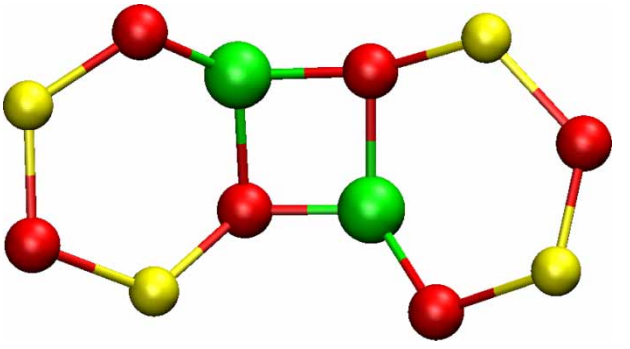

Figure 13. Local configuration of ZnO confined in a carbon nanotube. The red spheres are the oxygen atoms. Yellow and green spheres are the Zn atoms involved in a six-ring (wurtzite-type) configuration and a four-ring (rocksalt- or blende-type) configuration, respectively. The C atoms of the carbon nanotube are not shown for the sake of clarity (colour online).

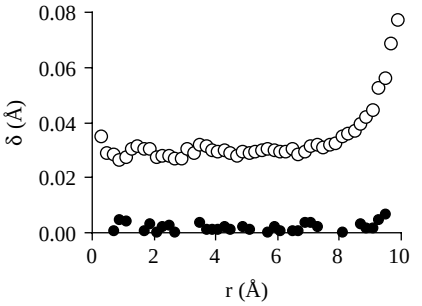

Figure 14. Radial distribution of the core-shell distances (dipole) for oxygen atoms in ZnO confined in a carbon nanotube with $D = 2.6$ nm (the filling density is $\rho = \rho_0$). The white and black symbols are the core-shell distances along the radial distance (r) and the pore axis (z), respectively.

case, the Zn atoms obeying this criterion are found to be part of a four-atom ring (Zn–O–Zn–O). Such Zn atoms were already mentioned in Section 4.1 in which we found that some atoms are involved in four-atom rings or in nanodomains of a cubic symmetry. The latter result is also consistent with the fact that the typical nearest neighbour distance of 2.9 Å for these atoms is very close to that observed in the case of the blende structure (see Figure 1 and Table 3), which is a cubic phase involving four-atom rings. In contrast, other Zn atoms (for which the Zn–Zn nearest neighbour distance falls in the main peak centred at about 3.2 Å) are involved in six-atom rings, as expected for a hexagonal wurtzite-like structure (Zn–O–Zn–O–Zn–O). The two situations are illustrated in the local molecular configuration that we isolated for that purpose in Figure 13.

In order to further characterise the nanoparticles obtained in the present work, we studied the polarity of their surface and the distribution of dipoles carried by the O atoms (core-shell model). Such results provide useful information regarding the physical, chemical and electronic properties of particles that can be obtained using porous materials as a template. Density profiles (not shown) show that all of the nanoparticles in this work exhibit neutral faces, i.e. faces terminated with both Zn and O atoms in the same stoichiometry (in contrast to polar surfaces terminated by a plane composed entirely of atoms of the same species). This is due to the symmetry of the cylindrical nanopore that imposes that the Zn and O atoms must be distributed equally along the radial direction. This prevents the system from having surfaces of different polarities (the same argument also holds for a slit pore). Figure 14 shows the radial distribution of dipoles carried by the O atoms. Both the contributions along the radial dimension (r) and the pore axis (z) are reported. No polarisation of the O atoms is observed along the pore axis as the core-shell distance Δz along z is close to zero. In contrast, the polarisation Δr along the radial direction r is non-negligible and positive. This result shows that the O atoms of the confined ZnO nanoparticles are polarised towards the external free interface (although the nanoparticles exhibit basal surfaces overall). In addition, the absolute value of the polarisation of the O atoms along the radial direction increases with increasing r. Such an increasing polarisation of the O atoms as they approach the external surface is due to the cost in free energy close to the interface that needs to be compensated by a decrease in the energy of the nanoparticle (the stability of the nanoparticle is assured by lowering the electrostatic energy).

5. Discussion and conclusion

This work provides insights into the microscopic properties of zinc oxide nanostructures obtained within the porosity of host carbon nanotubes. None of the nanostructures exhibits the ideal structure of one of the ZnO bulk crystal phases (rocksalt, blende and wurtzite), although they possess the local ordering of wurtzite with significant correlations for the first and second nearest neighbours. Each of the nanoparticles also exhibits some defects such as Zn atoms involved in four-member ring Zn–O–Zn–O (while Zn atoms in wurtzite are involved in six-member ring). As a result, in some cases, we also observe that the confined ZnO particle is composed of a mixture of hexagonal and cubic nanodomains. This result is consistent with the experimental work by Seo et al. [22]. These authors showed by means of field-emission scanning electron microscopy and X-ray diffraction that ZnO nanoparticles obtained within the channels of porous alumina have polycrystalline structural properties. The observation of different possible crystalline phases is also consistent with the work of Kulkarni et al. [33,34] who found that crystalline phase transitions in ZnO nanowires occur under uniaxial tensile loading. In the case of confined nanoparticles such as those reported in the present work, the interaction with the pore surface introduces an anisotropic constraint on the nanostructure, which may trigger transformations similar to those reported by Kulkarni et al. Finally, shifts in the relative stability of crystalline phases upon confinement are also in agreement with experiments by Meyer et al. [51] and molecular simulations by Wilson [50] on confined salts showing that freezing occurs at a temperature different from the bulk and that phase stability is affected by confinement. The results obtained in the present work are also in agreement with the experimental work by Polarz et al. [31] who studied ZnO nanoclusters confined in the pores of a host silica porous material by means of X-ray diffraction and EXAFS. In agreement with our results on the effect of nanotube diameter on the structure of confined ZnO nanoparticles, these authors showed that the degree of crystallinity of the synthesised nanostructure decreases as the pore size decreases (see figure 7 in [31]). Polarz et al. [31] also found that ZnO nanoparticles obtained for a nanopore of a diameter of $D = 1.8$ nm is

nearly amorphous and exhibits much less long-range crystalline order, in agreement with our results for a nanotube of a diameter $D = 1.8$ nm.

In agreement with our previous work on ZnO confined in porous silica, the morphology of the nanostructures embedded in the carbon nanotubes is found to depend on the different parameters involved in the synthesis (pore size and filling density). This result is consistent with the work by Shen et al. [49] who investigated the stability of small 1D ZnO nanostructures using *ab initio* calculations. These authors found that the nanorod (filled particle) has a lower energy (more stable) than the nanotube (hollow particle) when it is composed of a number of atoms larger than 38 (the smallest ZnO particle in the present work has 216 atoms). In the case of the carbon nanotube with $D = 2.6$ nm, we found that ZnO forms nanorods (quasi-1D systems) for all filling densities. In contrast, the morphology of the nanostructure in the case of the nanotube with the smaller diameter $D = 1.8$ nm depends on the filling density of the porosity. ZnO arranges itself to form nanorods (quasi-1D systems) for $\rho = 0.5\rho_0$ and ρ_0, while a nanoparticle (dimensionality '0D') is observed for $\rho = 0.30\rho_0$.

Due to the weak (only dispersive) attractive interactions between the carbon and the Zn and O atoms, the energy of the nanostructures after the removal of the host material is nearly equal to that of the embedded nanostructure. This result is consistent with the fact that the pair correlation functions $g(r)$ for the free structures relaxed before and after the removal of the host material are almost identical. It is also found that, independently of the carbon nanotube diameter, the ZnO–ZnO contribution to the energy decreases (becomes more attractive) as the number of ZnO monomers in the system increases. This result reflects that the surface to volume ratio decreases when the nanotube size increases or when the number of ZnO monomers increases. Finally, for all nanostructures, the energy per ZnO monomer remains smaller than the typical energy in bulk ZnO (~ -39.4 eV/ZnO). Our results also suggest that the energy of the nanoparticles is independent of the substrate as the data for carbon nanotubes and those from our previous work with silica nanopores almost fall on the same master curve.

All of the nanoparticles obtained in this work exhibit neutral faces, i.e. faces terminated with both Zn and O atoms in the same stoichiometry (in contrast to polar surfaces terminated by a plane composed entirely of atoms of the same species). We show that this is due to the symmetry of the cylindrical nanopore that imposes that the Zn and O atoms must be distributed equally along the radial direction. This prevents the system from having surfaces of different polarities (the same argument also holds for a slit pore). We also show that the O atoms are polarised along the radial direction $\Delta r > 0$ (i.e. towards the external free interface), while $\Delta z \sim 0$. In addition, the absolute value of the polarisation of the O atoms along the radial direction increases with increasing r, due to the cost in free energy close to the interface that needs to be compensated by a decrease in the energy of the nanoparticle.

Acknowledgements

The molecular simulations were performed on local workstations purchased thanks to the ANR research project 'SIMONAN-OMEM' (ANR-07-NANO-055) and the CNRS-ATILH Contrat de Programme de Recherche: Résistance, Porosité et Transport des Matériaux Cimentaires.

References

[1] Z.R. Tian, J.A. Voigt, J. Liu, B. Mckenzie, M.J. Mcdermott, M.A. Rodriguez, H. Konishi, and H. Xu, *Complex and oriented ZnO nanostructures*, Nat. Mater. 2 (2003), pp. 821–826.

[2] Y. Li, G.W. Meng, L.D. Zhang, and F. Phillipp, *Ordered semiconductor ZnO nanowire arrays and their photoluminescence properties*, Appl. Phys. Lett. 76 (2000), pp. 2011–2013.

[3] S. Iijima, *Helical microtubules of graphitic carbon*, Nature 354 (1991), pp. 56–58.

[4] P.M. Ajayan, *Nanotubes from carbon*, Chem. Rev. 99 (1999), pp. 1787–1799.

[5] L.D. Gelb, K.E. Gubbins, R. Radhakrishnan, and M. Sliwinska-Bartkowiak, *Phase separation in confined systems*, Rep. Prog. Phys. 62 (1999), pp. 1573–1659.

[6] C. Alba-Simionesco, B. Coasne, G. Dosseh, G. Dudzia, K.E. Gubbins, R. Radhakrishnan, and M. Sliwinska-Bartkowiak, *Effects of confinement on freezing and melting*, J. Phys. Condens. Matter 18 (2006), pp. R15–R68.

[7] C. Klingshirn, *ZnO: Material, physics and applications*, Chem. Phys. Chem. 8 (2007), pp. 782–803.

[8] A.B. Djurisic and Y.H. Leung, *Optical properties of ZnO nanostructures*, Small 2 (2006), pp. 944–961.

[9] C. Klingshirn, *ZnO: From basics towards applications*, Phys. Stat. Sol. B 244 (2007), pp. 3027–3073.

[10] Z.L. Wang, *The new field of nanopiezotronics*, Mater. Today 10 (2007), pp. 20–28.

[11] L. Schmidt-Mende and J.L. MacManus-Driscoll, *ZnO – nanostructures, defects, and devices*, Mater. Today 10 (2007), pp. 40–48.

[12] K. Matsumoto, K. Konemura, and G. Shimaoka, *Crystal-growth of ZnO by vapor transport in a closed tube using Zn and $ZnCl_2$ as transport agents*, J. Cryst. Growth 71 (1985), pp. 99–103.

[13] Y. Ishikawa, Y. Shimizu, T. Sasaki, and N. Koshizaki, *Preparation of zinc oxide nanorods using pulsed laser ablation in water media at high temperature*, J. Coll. Interface Sci. 300 (2006), pp. 612–615.

[14] J. Zhao, Z.G. Jin, T. Li, and X.X. Liu, *Preparation and characterization of ZnO nanorods from NaOH solutions with assisted electrical field*, Appl. Surf. Sci. 252 (2006), pp. 8287–8294.

[15] M. Krunks, T. Dedova, and I. Oja Acik, *Spray pyrolysis deposition of zinc oxide nanostructured layers*, Thin Solid Films 515 (2006), pp. 1157–1160.

[16] A.R. Boccaccini, J.A. Roether, B.J.C. Thomas, M.S.P. Shaffer, E. Chavez, E. Stoll, and E.J. Minay, *The electrophoretic deposition of inorganic nanoscaled materials*, J. Ceram. Soc. Jpn 114 (2006), pp. 1–14.

[17] Y. Hu and J.F. Chen, *Synthesis and characterization of semiconductor nanomaterials and micromaterials via gamma-irradiation route*, J. Cluster Sci. 18 (2007), pp. 371–387.

[18] O.P. Tkachenko, K.V. Klementiev, E. Loffler, I. Ritzkopf, F. Schuth, M. Bandyopadhyay, S. Grabowski, H. Gies, V. Hagen, M. Muhler, L. Lu, R.A. Fischere, and W. Grunert, *The structure of zinc and copper oxide species hosted in porous siliceous matrices*, Phys. Chem. Chem. Phys. 5 (2003), pp. 4325–4334.

[19] C. Bouvy, W. Marine, R. Sporken, and B.L. Su, *Nanosized ZnO confined inside a Faujasite X zeolite matrix: Characterization and optical properties*, Coll. Surf. A 300 (2007), pp. 145–149.

[20] R.G. Singh, F. Singh, V. Agarwal, and R.M. Mehra, *Photoluminescence studies of ZnO/porous silicon nanocomposites*, J. Phys. D: Appl. Phys. 40 (2007), pp. 3090–3093.
[21] W. Chen, X. Tao, Y. Liu, X. Sun, Z. Hu, and B. Fei, *Facile route to high-density, ordered ZnO nanowire arrays and their photoluminescence properties*, Appl. Surf. Sci. 252 (2006), pp. 8683–8687.
[22] B.I. Seo, U.A. Shaislamov, M.H. Ha, S.W. Kim, H.K. Kim, and B. Yang, *ZnO nanotubes by template wetting process*, Phys. E 37 (2007), pp. 241–244.
[23] T. Wagner, T. Waitz, J. Roggenbuck, M. Froba, C.D. Kohl, and M. Tiemann, *Ordered mesoporous ZnO for gas sensing*, Thin Solid Films 515 (2007), pp. 8360–8363.
[24] W.H. Zhang, J.L. Shi, L.Z. Wang, and D.S. Yan, *Preparation and characterization of ZnO clusters inside mesoporous silica*, Chem. Mater. 12 (2000), pp. 1408–1413.
[25] S.E. Dapurkar, S.K. Badamali, and P. Selvam, *Nanosized metal oxides in the mesopores of MCM-41 and MCM-48 silicates*, Catalysis Today 68 (2001), pp. 63–68.
[26] G.Q. Tang, Y. Xiong, L.Z. Zhang, and G.L. Zhang, *Novel long-lifetime photoluminescence of nanosized ZnO included in the mesoporous MCM-41*, Chem. Phys. Lett. 395 (2004), pp. 97–102.
[27] H.G. Chen, J.L. Shi, H.R. Chen, J.N. Yan, Y.S. Li, Z.L. Hua, Y. Yang, and D.S. Yan, *The preparation and photoluminescence properties of ZnO-MCM-41*, Opt. Mater. 25 (2004), pp. 79–84.
[28] F. Schroder, S. Hermes, H. Parala, T. Hikov, M. Muhler, and R. Fischer, *Non aqueous loading of the mesoporous siliceous MCM-48 matrix with ZnO: A comparison of solution, liquid and gas-phase infiltration using diethyl zinc as organometallic precursor*, J. Mater. Chem. 16 (2006), pp. 3565–3574.
[29] L.I. Burova, D.I. Petukhov, A.A. Eliseev, A.V. Lukashin, and Y.D. Tretyakov, *Preparation and properties of ZnO nanoparticles in the mesoporous silica matrix*, Superlatt. Microstruct. 39 (2006), pp. 257–266.
[30] Q. Jiang, Z.Y. Wu, Y.M. Wang, Y. Cao, C.F. Zhou, and J.H. Zhu, *Fabrication of photoluminescent ZnO/SBA-15 through directly dispersing zinc nitrate into the as-prepared mesoporous silica occluded with template*, J. Mater. Chem. 16 (2006), pp. 1536–1542.
[31] S. Polarz, F. Neues, M.W.E. van den Berg, W. Grunert, and L. Khodeir, *Mesosynthesis of ZnO-silica composites for methanol nanocatalysis*, J. Am. Chem. Soc. 127 (2005), pp. 12028–12034.
[32] A. Jentys and R.W. Grimes, *Embedding nano-clusters in siliceous faujasite*, J. Chem. Soc. Faraday Trans. 92 (1996), pp. 2093–2097.
[33] A.J. Kulkarni, M. Zhou, and F. Ke, *Orientation and size dependence of the elastic properties of zinc oxide nanobelts*, Nanotechnology 16 (2005), pp. 2749–2756.
[34] A.J. Kulkarni, M. Zhou, K. Sarasamak, and S. Limpijumnong, *Novel phase transformation in ZnO nanowires under tensile loading*, Phys. Rev. Lett. 97 (2006), 105502.
[35] B.G. Dick and A.W. Overhauser, *Theory of the dielectric constants of alkali halide crystals*, Phys. Rev. 112 (1958), pp. 90–103.
[36] G.W. Lewis and C.R.A. Catlow, *Potential models for ionic oxides*, J. Phys. C 18 (1985), pp. 1149–1161.
[37] A. Zaoui and W. Sekkal, *Pressure-induced softening of shear modes in wurtzite ZnO: A theoretical study*, Phys. Rev. B 66 (2002), 174106.
[38] R.A. Jackson and C.R.A. Catlow, *Computer simulation studies of zeolite structure*, Mol. Simul. 1 (1988), pp. 207–224.
[39] J.S. Rowlinson, *Liquids and Liquid Mixtures*, Butterworth Scientific, London, 1982.
[40] H. Partridge, J.R. Stallcop, and E. Levin, *Potential energy curves and transport properties for the interaction of He with other ground-state atoms*, J. Chem. Phys. 115 (2001), pp. 6471–6488.
[41] D. Nicholson and N.G. Parsonage, *Computer Simulation and the Statistical Mechanics of Adsorption*, Academic Press, New York, 1982.
[42] M.P. Allen and D.J. Tildesley, *Computer Simulation of Liquids*, Clarendon, Oxford, 1987.
[43] D. Frenkel and B. Smit, *Understanding Molecular Simulation: From Algorithms to Applications*, 2nd ed., Academic Press, London, 2002.
[44] B. Coasne, J. Czwartos, K.E. Gubbins, F.R. Hung, and M. Sliwinska-Bartkowiak, *Freezing and melting of binary mixtures confined in a nanopore*, Mol. Phys. 102 (2004), pp. 2149–2163.
[45] J. Czwartos, B. Coasne, K.E. Gubbins, F.R. Hung, and M. Sliwinska-Bartkowiak, *Freezing and melting of azeotropic mixtures confined in nanopores: Experiment and molecular simulation*, Mol. Phys. 103 (2005), pp. 3103–3113.
[46] B. Coasne, S.K. Jain, and K.E. Gubbins, *Freezing of fluids confined in a disordered nanoporous structure*, Phys. Rev. Lett. 97 (2006), 105702.
[47] J.E. Jaffe and A.C. Hess, *Hartree-Fock of phase changes in ZnO at high pressure*, Phys. Rev. B 48 (1993), pp. 7903–7909.
[48] B. Coasne, A. Mezy, R.J.M. Pellenq, D. Ravot, and J.C. Tedenac, *Zinc oxide nanostructures confined in porous silicas*, J. Am. Chem. Soc. 131 (2009), pp. 2185–2198.
[49] X. Shen, P.B. Allen, J.T. Muckerman, J.W. Davenport, and J.C. Zheng, *Wire versus tube: stability of small one-dimensional ZnO nanostructures*, Nano Lett. 8 (2007), pp. 2267–2271.
[50] M. Wilson, *The formation of low-dimensional ionic crystallites in carbon nanotubes*, J. Chem. Phys. 116 (2002), pp. 3027–3041.
[51] R.R. Meyer, J. Sloan, R.E. Dunin-Borkowski, A.I. Kirkland, M.C. Novotny, S.R. Bailey, S.R. Hutchinson, and L.M.H. Green, *Discrete atom imaging of one-dimensional crystals formed within single-walled carbon nanotubes*, Science 289 (2000), pp. 1324–1326.